Journal of Power Sources 324 (2016) 729–737

Contents lists available at ScienceDirect

Journal of Power Sources

journal homepage: www.elsevier.com/locate/jpowsour

Load cycle durability of a graphitized carbon black-supported platinum catalyst in polymer electrolyte fuel cell cathodes

Chikara Takei [a], Katsuyoshi Kakinuma [b], Kazuhito Kawashima [a], Keisuke Tashiro [a], Masahiro Watanabe [b], Makoto Uchida [b, *]

[a] Advanced Powertrain Development, Mitsubishi Motors Corporation, 1 Nakashinkiri, Hashime-cho, Okazaki, Aichi, 444-8501, Japan
[b] Fuel Cell Nanomaterials Center, University of Yamanashi, 6-43 Miyamae, Kofu, Yamanashi, 400-0021, Japan

HIGHLIGHTS

- The degradation of Pt is suppressed by FCV drive cycles with short OCV holding times.
- The oxidation of Pt depends on the OCV holding time and RH.
- Load cycles with long OCV accelerate Pt dissolution in the CL near the membrane.
- Load cycles with low current density accelerate the Pt particle growth.
- Load cycles at low RH suppress the dissolution and particle growth of Pt.

GRAPHICAL ABSTRACT

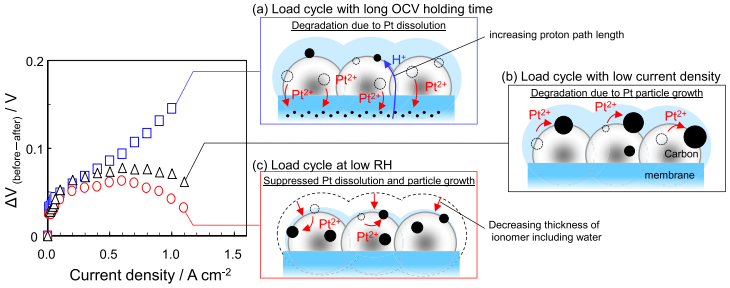

ARTICLE INFO

Article history:
Received 2 April 2016
Received in revised form
21 May 2016
Accepted 24 May 2016
Available online 6 June 2016

Keywords:
Polymer electrolyte fuel cells
Load cycle
Graphitized carbon black-supported platinum catalyst
OCV/load holding time
Pt dissolution
Pt particle growth

ABSTRACT

We focus on Pt degradation occurring during fuel cell vehicle (FCV) combined drive cycles involving load and open circuit voltage (OCV) just after startup and during idling. Load cycle durability is evaluated as a function of OCV/load holding time, load rate and relative humidity (RH) with a graphitized carbon black-supported platinum catalyst (Pt/GCB) in the cathode. The degradation of Pt/GCB is suppressed for shorter OCV holding times, lower load rates and lower RH. Scanning ion microscopy (SIM) images of membrane cross-sections indicate that the amount of Pt deposited in the membrane decreases during drive cycles involving load with short OCV holding times. Investigations of the Pt distribution in the cathode catalyst layer (CL) by using scanning TEM-EDX show that the dissolution of Pt is suppressed on the membrane side in the CL. The Pt dissolution is accelerated by the high Pt oxidation due to the long OCV holding time. A load cycle with both long OCV holding time and low load inhibits the Pt^{2+} migration into the membrane but accelerates the Pt particle growth due to electrochemical Ostwald ripening; meanwhile, a load cycle with long OCV holding time at lower RH prevents both the Pt dissolution and particle growth.

1. Introduction

Polymer electrolyte fuel cells (PEFCs) used in fuel cell vehicles (FCV) are power generation devices with low environmental impact, having features such as high theoretical efficiency and zero CO_2 emissions. One of the main impediments to the expansion of the FCV market is the high cost of the FC engine system as compared to the internal-combustion engine, e.g., because the PEFC electrodes still require a large amount of Pt as the electrocatalyst. In addition, it is known that both the carbon-supported Pt

* Corresponding author.
E-mail address: uchidam@yamanashi.ac.jp (M. Uchida).

http://dx.doi.org/10.1016/j.jpowsour.2016.05.117

electrocatalyst and the membrane are degraded under various types of FCV operating conditions such as startup/shutdown [1–4], load cycling [5,6], and idling [7,8]. It is important to increase the durability of the electrocatalyst under these operating conditions in terms of decreasing the FCV life cycle cost. Therefore, we particularly focused on load cycling, which accelerates the degradation of the Pt nanoparticles (NPs). Since load cycling leads to the degradation of Pt NPs due to dissolution [9–11] and particle growth [12,13], many researchers have been trying to resolve this issue. It is well known that the degradation of Pt NPs is evaluated by potential cycling, which simulates load cycling, using a potentiostat. The degradation of Pt has been intensively investigated under various potential cycling conditions by Mitsushima et al. [14–17]. According to these papers, the degradation of Pt under potential cycling is accelerated by a high positive-going rate and a low negative-going rate [15], increasing temperature and decreasing pH [16]. Moreover, other researchers have also reported the degradation of Pt under various potential cycling regimes [18–20]. Uchimura et al. have reported that the degradation of Pt was accelerated to a greater extent under potential cycling involving asymmetric triangular profiles with lower negative-going rates compared with those with low positive-going rates [18]. Yasuda et al. found that Pt deposition in the membrane was accelerated by the presence of hydrogen transported through the membrane from the anode. This deposition was also affected by the presence of oxygen in the cathode [20]. Kongkanand et al. also concluded that the electrooxidation of Pt is accelerated more by the presence of oxygen than the presence of nitrogen at lower potentials [21]. The degradation of Pt NPs under potential cycling is primarily caused by Ostwald ripening and place exchange. Ostwald ripening leads to increased Pt particle size, because the smaller particles have a higher surface energy and thus are less stable than the larger particles [5,17,20,22]. Oxygen atoms adsorbed on the Pt surface can enter the Pt lattice by place exchange at potentials greater than 1.1 V [23–26]. These studies have revealed that the degradation of Pt during potential cycling is correlated strongly with the oxidation of Pt NPs. However, it has been suspected that the actual degradation of Pt is different from that observed with potential cycling with H_2/N_2, because the FCV operating condition includes load cycling with H_2/air.

In this research, we investigated the degradation of the electrocatalyst in terms of Pt dissolution, Pt deposition, and Pt particle growth in both the catalyst layer (CL) and membrane under various load cycle conditions, as a function of the open circut voltage (OCV)/load holding time, current density range, and RH. Electrochemical evaluation was carried out with cyclic voltammetry (CV) and current–potential (*I–E*) polarization curve measurements. The electrodes were analyzed by transmission electron microscopy (TEM), scanning ion microscopy (SIM) and scanning transmission electron microscopy–energy dispersive X-ray spectroscopy (STEM-EDX) before and after the load cycling evaluations. These results provide information on the degradation of Pt under realistic FCV operating conditions.

2. Experimental

2.1. Preparation of membrane-electrode assembly (MEA)

Uniformly catalyst-coated membranes (CCM) were prepared in the same manner as in our previous research [3,4]. The catalyst pastes were prepared with 30 wt% Pt-loaded graphitized carbon black for the cathode (Pt/GCB, TEC10EA30E, Tanaka Kikinzoku Kogyo K. K.) or 46 wt% Pt-loaded carbon black for the anode (Pt/CB, TEC10E50E, Tanaka Kikinzoku Kogyo K. K.), mixed with ionomer (ion exchange capacity, IEC = 0.99 meq g^{-1}, Nafion ionomer DE521, E. I. Du Pont de Nemours & Co., Inc.), ethanol, and pure water by use of a planetary ball mill (P-6, Fritsch GmbH) for 30 min. The mass ratio of Nafion binder (dry basis) to carbon black (Nafion binder/carbon) was adjusted to 0.7. To prepare the uniform CCM, the catalyst pastes were directly sprayed onto a Nafion membrane maintained at 55 °C (NRE 211, 25 μm thickness, E. I. Du Pont de Nemours & Co., Inc.) with the pulse-swirl-spray technique (PSS, Nordson Co. Ltd.), and then dried at 60 °C in an electric oven. The CCMs were annealed by hot-pressing at 140 °C and 1.0 MPa for 3 min, and then they were assembled with two gas diffusion layers (GDLs, 25BCH, SGL Carbon Group Co., Ltd.) and a single serpentine pattern cell (Japan Automobile Research Institute (JARI) standard cell) with an active geometric area of 29.2 cm^2. The Pt loading of the cathode CLs was 0.10 ± 0.006 mg-Pt cm^{-2}, and the Pt loading of the anode CLs was 0.50 ± 0.025 mg-Pt cm^{-2}.

2.2. MEA characterization

The cell was operated with hydrogen and oxygen/air at 80 °C under ambient pressure (1 atm). Hydrogen gas was supplied to the anode and oxygen/air to the cathode. The flow rates of all gases were controlled by mass flow controllers. The utilizations of the reactant gases were 70% for H_2, 40% for O_2 and 40% for air. These gases were humidified at various levels of humidification by bubbling through a heated water reservoir. The cell potential (*E*) was measured as a function of current density by use of an electronic load (PLZ-664WA, Kikusui Electronics Co.) operated in the constant current mode, controlled by a measurement system (AB-3520AS001, Panasonic Production Technology Co., Ltd.). The cell resistance was measured at 1 kHz under load by use of a digital ac milliohmmeter (Model 3566, Tsuruga Electric Co.). The *I–E* curves were measured during quasi-steady-state operation achieved after 5 min at each potential step. For experimental convenience, the hydrogen anode was used as the reference electrode for both MEA polarization and CV measurements, since the polarization of the hydrogen anode was relatively small, even at high current density. To evaluate the electrochemically active surface area (ECSA) of the Pt catalyst in the cathode layer, CV measurements were performed at 80 °C and 100% RH by use of a potentiostat (HZ-5000, Automatic Polarization System, Hokuto Denko Co.). The cathode compartment was purged with N_2 (100 mL min^{-1}, 100% RH), while H_2 gas (100 mL min^{-1}, 100%-RH) was supplied to the anode. Prior to the sweep, the potential was maintained at 0.075 V for 3 s to ensure that the Pt was in a reproducibly reduced state. Then, the potential was swept from 0.075 V to 1.000 V at 20 mV s^{-1} and reversed back to 0.075 V. The electrical charge for H^+ reduction to adsorbed H was calculated from the current flowing in the negative-going potential sweep in the range from ca. 0.4 V vs. RHE to 0.075 V at the cathode, with subtraction of the estimated double layer charging current [3,4]. The entire CV was measured without N_2 flow to avoid perturbing the H_2 partial pressure [27]. The value of ECSA was determined from the hydrogen adsorption charge referred to Q_H^o = 0.21 mC cm^{-2}, the conventional value for a monolayer of adsorbed hydrogen on polycrystalline platinum [28].

2.3. Durability evaluations in load cycles

Fig. 1(a) shows the protocol for the evaluation of the durability of the Pt/GCB cathode catalysts in the current-load mode. Table 1 shows the details of the protocols employing various load cycling conditions involving OCV and load holding times at a high current density (sample names A1, A2 and A3), at a lower current density (A5) and at OCV (A4) under 100% RH and a lower RH (A6). These durability evaluation protocols can be characterized as follows: A1, with the OCV/load holding times of 3 s/3 s, simulates a normal acceleration/deceleration drive cycle; A2, with the OCV/load

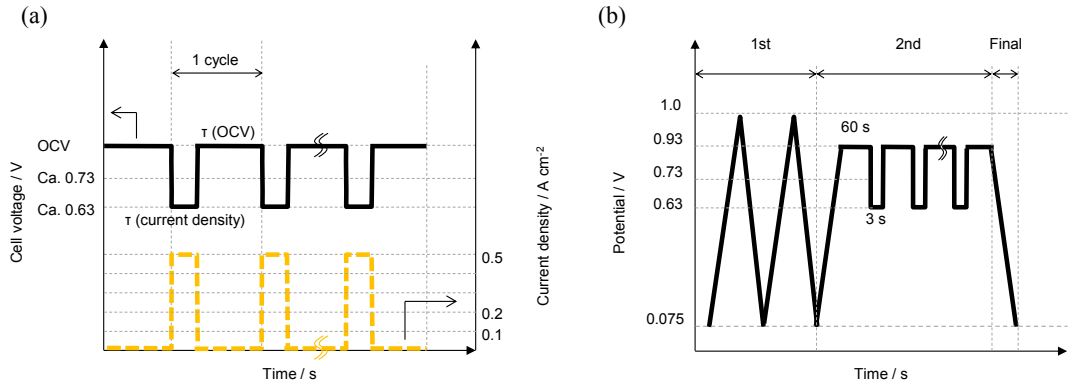

Fig. 1. (a) Protocol for the simulation of fuel cell load cycles with OCV and various current loads (0, 0.1, 0.2, 0.5 A cm^{-2}) with supply of H_2/air at either 50 or 100% RH; holding time at OCV, τ(OCV) = 3, 60 and 600,000 s, and holding time under current load, τ(CL) = 0, 3 and 60 s. (b) Simulated load cycle protocol in potentiostatic mode.

Table 1
Load cycle conditions.

Sample name	Nominal cell potential range (V)	OCV holding time (s)	Load current density (A cm^{-2})	Load holding time (s)	Cycle number	Total OCV holding time (s (min))	Relative humidity, (% RH)
A1	ca. 0.63 ↔ OCV	3	0.5	3	10,000	30,000 (500)	100
A2	ca. 0.63 ↔ OCV	3	0.5	60	10,000	30,000 (500)	100
A3	ca. 0.63 ↔ OCV	60	0.5	3	10,000	600,000 (10,000)	100
A4	OCV	600,000	0.0	0	–	600,000 (10,000)	100
A5	ca. 0.73 ↔ OCV	60	0.1	3	10,000	600,000 (10,000)	100
A6	ca. 0.63 ↔ OCV	60	0.2	3	10,000	600,000 (10,000)	50

holding times of 3 s/60 s, simulates a high-speed drive cycle; A3, with the OCV/load holding times of 60 s/3 s simulates a high-frequency idling/drive cycle; A4, with OCV only, i.e., without a load cycle, simulates long-term idling; A5, with the OCV/load holding times of 60 s/3 s using low current density, simulates a possible strategy to suppress the degradation during load cycling in comparison with that using high current density, and A6, with the OCV/load holding times of 60 s/3 s at low RH, simulates a second possible strategy to suppress the degradation during load cycling in comparison with that at 100% RH. The durability evaluations were performed with H_2 (anode, 145 mL min^{-1}) and air (cathode, 604 mL min^{-1}) in the potential range from ca. 0.6 V to OCV at 80 °C and ambient pressure. In the first step, the initial *I-E* curves and CVs were measured. In the second step during the load cycling evaluations, the ECSA values of the cathode were examined every 2,000th cycle by CV. In the last step after the load cycling, the cell performances (*I-E* curves) were compared with the initial ones. In the post-analysis, the degradation of the Pt was observed by TEM. In addition, cross-sections of the MEAs were analyzed by two different methods. In the first, the deposition of Pt was observed in the membrane by scanning ion microscopy (SIM) in a focused ion beam system (FIB, FB-2200, Hitachi High-Technologies Co., Ltd.). In the second, the Pt distribution was observed in the cathode CL by STEM-EDX (HD-2700, Hitachi High-Technologies Co., Ltd.).

2.4. Pt oxidation characteristic during simulated load cycles by use of an actual potentiostat

Fig. 1(b) and Table 2 show the protocol and the conditions of the simulated load cycling carried out by use of an actual potentiostat, with H_2 (anode, 100 mL min^{-1}) and N_2 (cathode, 100 mL min^{-1}) atmospheres at 80 °C. In the first step, CV was carried out for 2 cycles at 20 mV s^{-1} to stabilize the electrocatalyst. In the second step, the simulated load cycles were performed at 240/0.1 V s^{-1} anodic/cathodic scan rates for 0, 12, 48, 100 cycles. In the final step, the reduction charge of PtO was measured by linear sweep voltammetry at 20 mV s^{-1} after various numbers of simulated load cycles. These conditions can be characterized as follows: B3 simulates the load cycle of A3 with the OCV/load holding times 60 s/3 s; B5 simulates a load cycle with low current density; and B6 simulates a load cycle at low RH in the potentiostatic mode, corresponding to the simulations under the current-load modes shown in Table 1 but replacing the OCV with the closed circuit potential 0.93 V.

3. Results and discussion

3.1. Effect of OCV/load holding time

Fig. 2(a) shows the normalized ECSA changes during the load cycling durability evaluations, which were operated with H_2 (anode) and air (cathode) atmosphere at 80 °C and 100% RH, as a function of the OCV/load holding time. The ECSA values of the cathodes for all MEAs (samples A1, A2, A3) decreased during cycling. In particular, the ECSA change of the A3 cell (OCV/load holding times 60 s/3 s), decreased drastically. In contrast, the decreases for both the A1 cell (OCV/load holding times 3 s/3 s) and the A2 cell (3 s/60 s) were significantly smaller than that for the A3 cell. Fig. 2(b) shows the IR-free polarization curves before and after the durability evaluations. The *I–E* curves were measured in H_2/air atmosphere at 80 °C and 100% RH. The cell performances for both A1 and A2 obtained after the durability evaluations were nearly the same as their initial performances, but that for A3 decreased markedly. In a comparison of the cell performances and the ECSA values, the decreasing ECSA values of about 20% under the A1 and A2 conditions do not affect the cell performances, whereas decreasing ECSA values of more than about 50% do affect the cell performances in Fig. 2(a), (b). Therefore, we found that the ECSA decrease of 20% does not significantly affect the oxygen reduction reaction. Fig. 2(c) shows the normalized ECSA changes occurring

Table 2
Potential cycling conditions.

Sample name	Potential range (V)	Lower potential holding time (s)	Higher potential holding time (s)	Cycle number	Relative humidity, % RH
B3	0.63 ↔ 0.93	3	60	0, 12, 48, 100	100
B5	0.73 ↔ 0.93	3	60	0, 12, 48, 100	100
B6	0.63 ↔ 0.93	3	60	0, 12, 48, 100	50

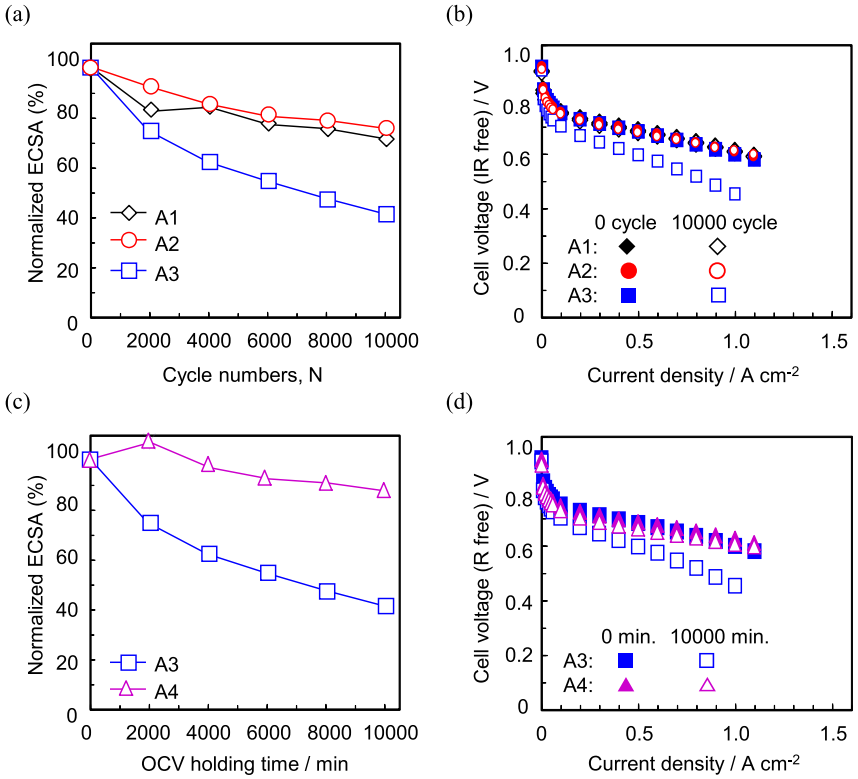

Fig. 2. (a) Normalized ECSA changes during the durability evaluations of load cycles with holding times of OCV/load (0.5 A cm^{-2}) between ca. 0.63 V and OCV at 80 °C and 100% RH, ◊: 3 s/3 s (A1), ○: 3 s/60 s (A2) □: 60 s/3 s (A3), (b) IR-free polarization curves before and after the durability evaluations at 80 °C and 100% RH under H_2/air, (c) Normalized ECSA changes during the load cycles and the OCV holding at 80 °C and 100% RH, □: OCV/load holding time of 60 s/3 s (A3), △: OCV holding time of 10,000 min (A4), (d) IR-free polarization curves before and after the load cycles and OCV holding at 80 °C and 100% RH under H_2/air.

during the durability evaluation A3 (OCV/load holding times 60 s/3 s) and A4 (OCV, without load) as a function of the accumulated OCV holding times for both durability evaluations. The decrease of ECSA for A4, without the load-cycling, was suppressed in comparison to that for A3. Fig. 2(d) shows the IR-free polarization curves before and after the durability evaluations. The cell performance for A4 did not decrease, but that for A3 did decrease noticeably, compared with their respective initial performances. These results indicate that the interim load cycles between the OCV holding periods clearly affected the degradation of the cathode electrocatalyst. This phenomenon corresponds to the previous results of our group, which reported the deleterious effects of interim CV on Pt/carbon black catalyst degradation during startup/shutdown cycling evaluation [4].

Fig. 3 shows TEM images of the Pt/GCB cathode catalyst before and after the durability evaluations with current load cycling. Comparing the images obtained for protocols with interim load cycles (b, c, d) and that obtained for a protocol without load cycling (e), it is clear that the Pt aggregation was enhanced by the interim load cycling. The mean particle size of the Pt/GCB cathode catalyst, which was 5.4 nm ± 2.3 nm after preconditioning (Fig. 3(a)), increased after the durability evaluations: (b) 7.7 nm ± 3.3 nm under A1 conditions; (c) 7.1 nm ± 2.3 nm under A2 conditions; (d) 7.5 nm ± 3.2 nm under A3 conditions; and (e) 6.6 nm ± 2.7 nm under A4 conditions. In the TEM image (d) for A3, it is quite clear that fewer Pt NPs were observed probably due to the dissolution and/or detachment from the GCB support, although a mean particle size similar to those for A1, A2 and A4 was maintained. These results are well consistent with the ECSA changes and *I-E* performances shown in Fig. 2. The distinctive performance degradation for A3 must not have been brought about by either the load time period (A2) or that of OCV (A4) independently but by the combination of both the load and the long OCV time periods (A1< A3).

Fig. 4 shows the SIM images of the MEA cross-sections produced using the focused ion beam after the durability evaluations. A few Pt particles were observed in the membranes for the A1, A2 and A4 cells in Fig. 4 (a), (b), (d), but a large number of Pt particles were observed in the membrane of the A3 cell in Fig. 4(c). The size of the Pt particles in the A3 membrane was larger than those of the others. The location of the deposited Pt particles was near the cathode side of the membrane. Since the anode potential had been held at the hydrogen potential, it is concluded that the deposited particles must have formed from the Pt dissolved from the cathode CL. These results also indicate that the degradation of the Pt/GCB cathode was enhanced in the A3 condition, again consistent with the results of Fig. 2.

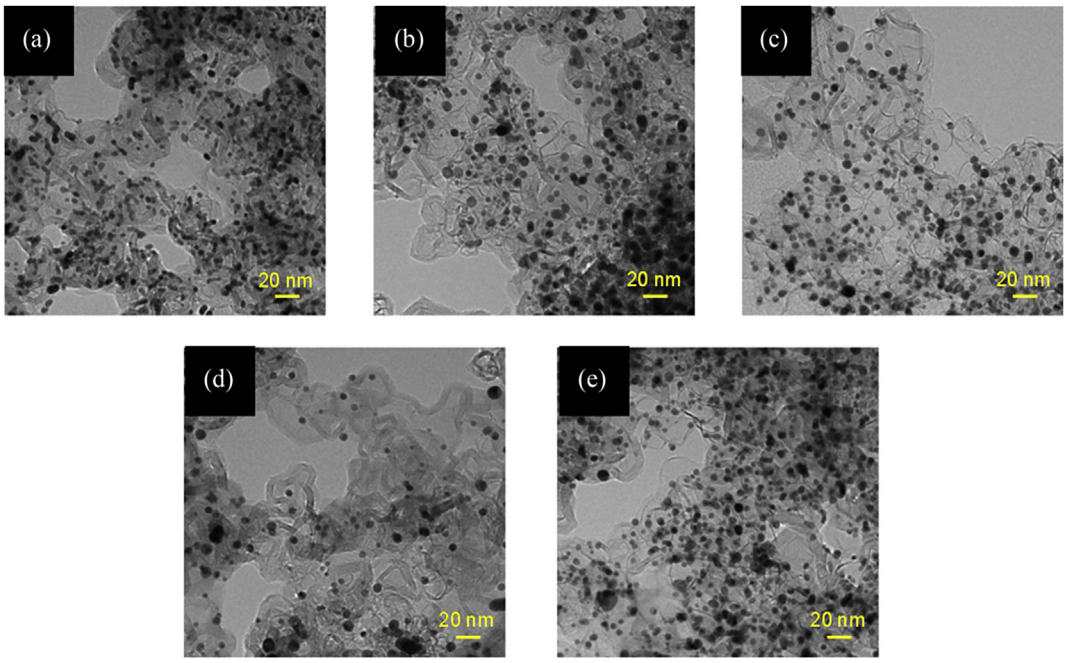

Fig. 3. TEM images of Pt/GCB cathode catalyst before and after the durability evaluations: (a) initial Pt/GCB cathode electrocatalyst after conditioning, (b) after the durability evaluation with holding times of OCV 3 s/load 3 s (A1), (c) OCV 3 s/load 60 s (A2), (d) OCV 60 s/load 3 s (A3), (e) OCV holding time of 10,000 min without load cycle (A4).

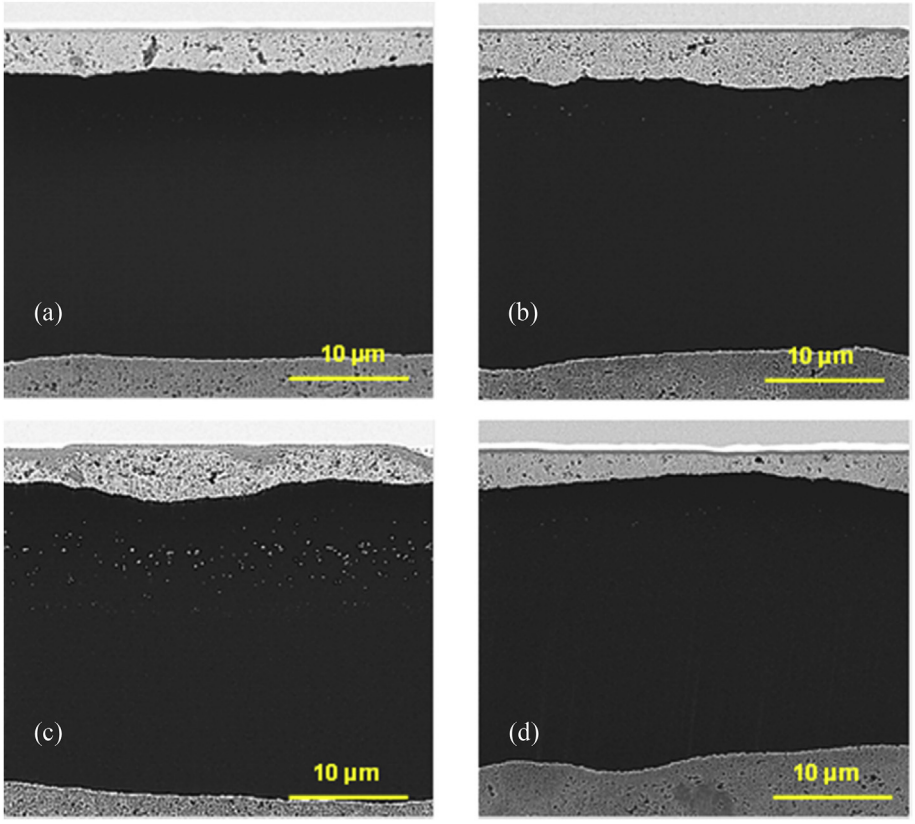

Fig. 4. SIM images of the cross-sections of MEAs after the durability evaluations: (a) with OCV/load holding times of 3 s/3 s (A1), (b) 3 s/60 s (A2), (c) 60 s/3 s (A3), (d) OCV holding time of 10,000 min (A4).

3.2. Effects of both the current density range and RH on the degradation of cathode electrocatalyst

The effects of both the current density range and RH on the MEA performance were investigated in order to try to find ways to suppress the degradation of the cathode electrocatalyst (Fig. 5). The A5 cell was operated in the constant current mode at the load current density 0.1 A cm^{-2} at 80 °C 100% RH in order to control the potential range between ca. 0.73 V and the OCV. The A6 cell was also operated at the load current density 0.2 A cm^{-2} at 80 °C 50% RH in order to control the potential range between 0.63 V and the OCV. These durability evaluations were all carried out with the OCV/load holding times of 60 s/3 s in order to accelerate the degradation of Pt, based on the results of Fig. 2. Fig. 5(a) shows the normalized ECSA changes during the durability evaluations in the low current density range (A5) and the low RH condition (A6), compared with the A3 condition (see Table 1). The ECSA changes for both A5 and A6 were smaller than that for A3 during the durability evaluation. The cell performances for both A5 and A6 were higher than that of A3 after the durability evaluation (Fig. 5(b)). The deterioration of the cell performances under conditions A5 and A 6 was particularly suppressed in the high current density region compared with that of A3 (Fig. 5(c)). The cell voltage difference under the A6 condition was smaller than that under the A5 condition. From these results it is clear that the degradation of the electrocatalyst under the load cycles with long OCV holding time (60 s) is able to be suppressed by decreasing the load current density, and was more effectively suppressed by lowering the RH.

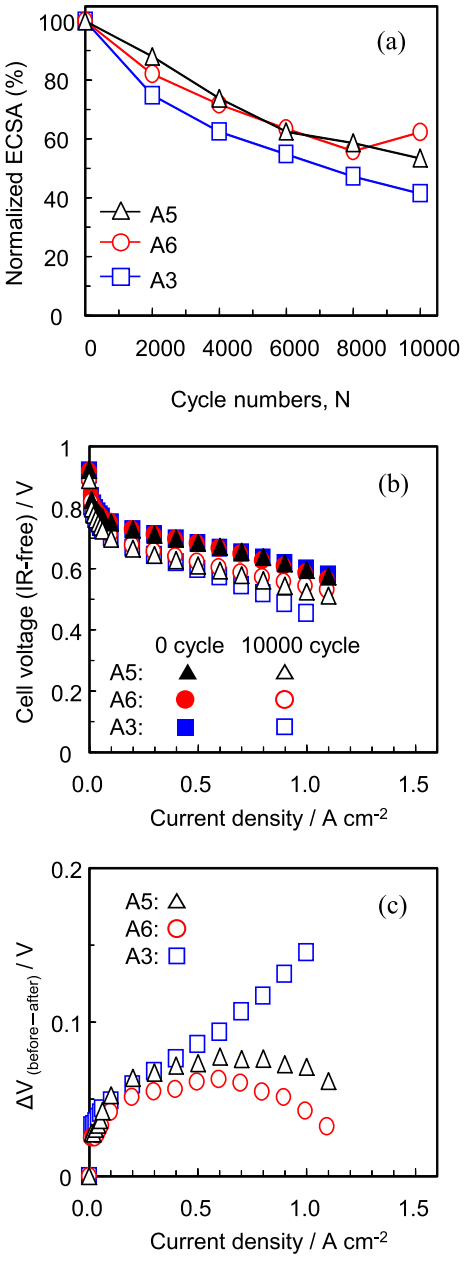

Fig. 5. (a) Normalized ECSA changes of the cathode during the durability evaluations using A3, A5, A6 conditions, □: load cycle with OCV/load holding times of 60 s/3 s (A3, ca. 0.63 V – OCV, 100% RH), △: load cycle with low current density (A5, ca. 0.73 V – OCV, 100% RH), ○: load cycle at low RH (A6, ca. 0.63 V – OCV, 50% RH), (b) IR-free polarization curves before and after the durability evaluations, (c) difference of cell voltages before and after the durability evaluations using A3, A5, A6 conditions.

Fig. 6(a–c) shows the Pt distribution in the cathode CL near the side of the membrane after the durability evaluations using the load cycles with long OCV hold time (a, A3), with low current density (b, A5), and at low RH (c, A6). The vertical axis shows the distance in the CL thickness direction, increasing from the membrane boundary at the bottom. The EDX line-scan for Pt in Fig. 6(a) shows that the Pt intensity decreased toward the membrane boundary. In the cases of Fig. 6 (b) and (c), the Pt intensity did not show such a trend. Therefore, the performances of the A5 and A6 cells in the high current density region, over 1.0 A cm^{-2} (Fig. 5(b)), were maintained at a high level, presumably because uniform reaction areas were retained, due to suppression of the Pt particle dissolution near the membrane boundary. Fig. 6(d–f) shows TEM images of the Pt particles on the GCB support and the Pt particle size distribution after the durability evaluations. The mean diameter of the Pt particles before the durability evaluation was 5.4 nm ± 2.3 nm (Fig. 3(a)). All of the particles increased in size as a result of the durability evaluation. The Pt particle size for the A6 cell was 7.1 nm ± 3.2 nm, which was significantly smaller than those for the other cells, i.e., 7.5 nm for A3 and 8.6 nm for A5. These results indicate that the degradation of the electrocatalyst in the case of the high current density range (A3, ca. 0.63 V – OCV) under the large amounts of crossover H_2 and back-diffusing water was preferentially caused by the Pt dissolution near the membrane boundary, and that in the case of low current density (A5, ca. 0.73 V – OCV) under the small amounts of crossover H_2 and back-diffusing water was preferentially caused by Pt particle growth. On the other hand, in the durability evaluation at low RH (A6) under the small amount of water, both the Pt dissolution and Pt particle growth were effectively suppressed.

3.3. Effects of both the lower potential limit and RH on the PtO reduction charge during simulated load cycles

Fig. 7(a) shows the effects of both the lower potential limit and RH on (a) the absolute PtO reduction charge (Q_{PtO}) and (b) the normalized Q_{PtO} changes of the Pt/GCB electrocatalyst during the three simulated load cycles using the potentiostat under H_2/N_2 atmosphere at 80 °C (B3, B5 and B6). The B3 condition corresponds to the load cycles of the A3 conditions between the OCV and 0.5 A cm^{-2} loading at 100% RH. The B5 condition does that of the A5 condition between the OCV and 0.1 A cm^{-2} loading at 100% RH by changing the lower potential limit to 0.73 V from 0.63 V. The B6 condition does that of the A6 condition between the OCV and 0.2 A cm^{-2} loading at 50% RH (OCV/load, 60 s/3 s, see Tables 1 and 2).

All of the Q_{PtO} values at 12 cycles were larger than the initial values but then decreased. The Q_{PtO} values increased in the order B6 < B3 < B5. These increases in the first stage up to 12 cycles

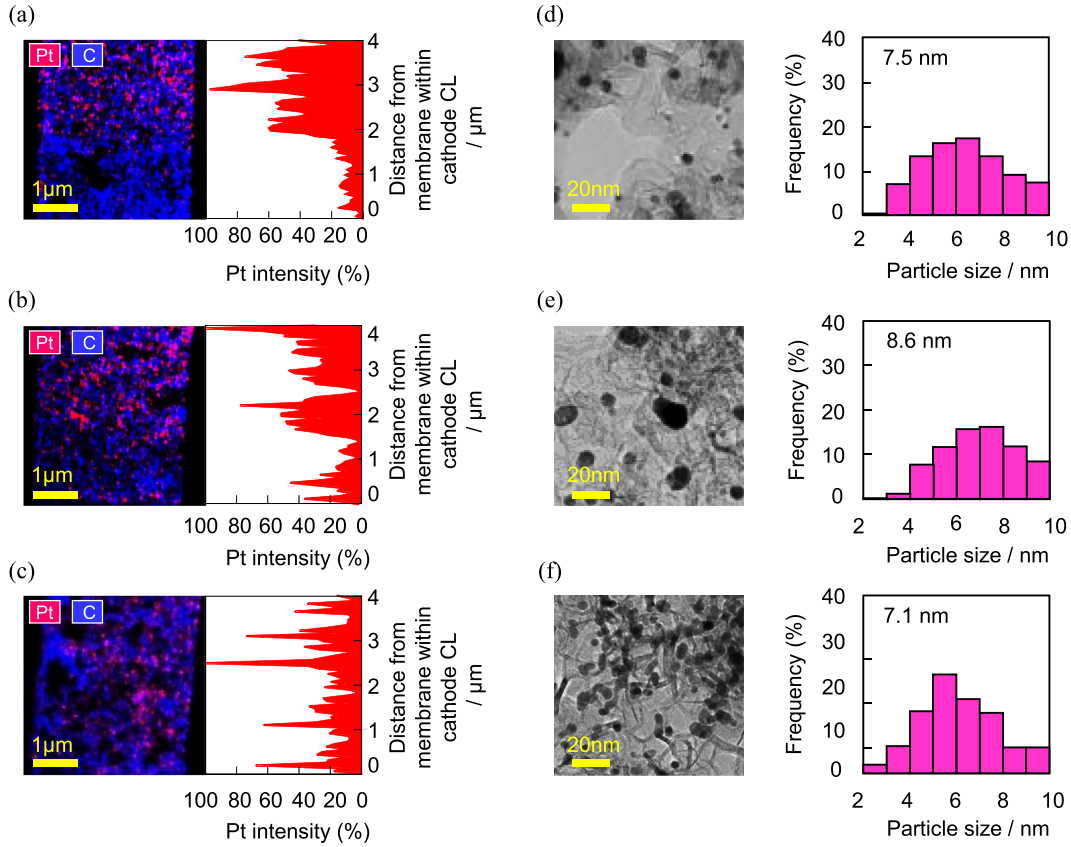

Fig. 6. Pt distribution by EDX element mapping (left) and Pt line scan (right) in the cathode CL near side of the membrane after the durability evaluations using (a) load cycle with long OCV holding time (A3), (b) with low current density (A5), and (c) at low RH (A6). The vertical axis shows the CL distance from the membrane. TEM images of Pt particles on GCB support (left) and particle size distribution of Pt (right) after the durability evaluations; (d) load cycles with long OCV holding time (A3), (e) with low current density (A5), and (f) at low RH (A6).

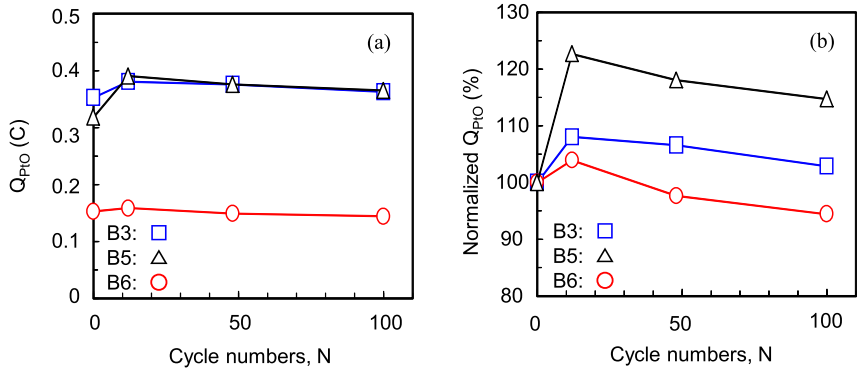

Fig. 7. Effects of both the low potential limit and RH on (a) absolute and (b) normalized PtO reduction charge during simulated load cycles using a potentiostat: △: with narrow potential range and high RH (B5, 0.73 V–0.93 V, 100% RH); ○: with wide potential range and low RH (B6, 0.63 V–0.93 V, 50% RH); □: with wide potential range and high RH (B3, 0.63 V–0.93 V, 100% RH).

indicate the degree of the Pt oxidation, and the decreases in the second stage thereafter then indicate the dissolution of Pt. In the case of the B5 condition (0.73 V–0.93 V, simulating A5), the Pt oxidation was enhanced compared with that of B3 (0.63 V–0.93 V, simulating A3) and was then maintained. Differences in the impact of each of the conditions (B3, B5 and B6) in terms of the Pt oxidation during the potential cycling were more clearly distinguishable with the normalized Q_{PtO} in Fig. 7(b). Therefore, these results indicate that the high potential operation (0.73 V) enhanced the Pt oxidation and also suppressed the Pt dissolution by the protection with the oxide film. In the case of the B6 condition (50% RH, simulating A6), the Q_{PtO} value was smaller than that for B3 (100% RH, simulating A3). This result suggests that the low RH condition suppressed both the Pt oxidation and the Pt dissolution.

3.4. Mechanisms and suppress conditions for the degradation of the cathode performance in the load cycles using current density

From all of the results of operating conditions, A1 to A6 and B3, B5, B6, we illustrate the models of both the Pt degradation and the

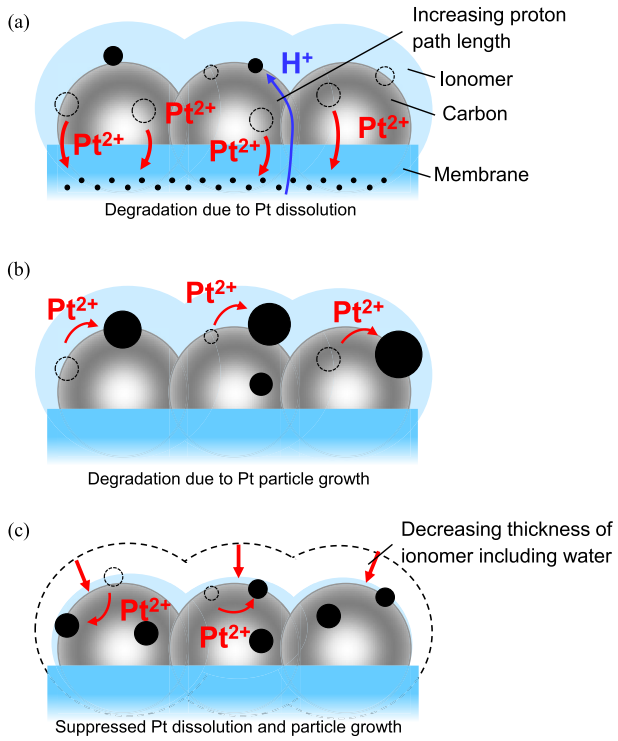

Fig. 8. Schematic of Pt (black) degradation on the GCB (gray) support in the cathode for (a) load cycles with a longer OCV holding time (A3, ca. 0.63 V – OCV, 100% RH), (b) that with a low current density range (A5, ca. 0.73 V – OCV, 100% RH), (c) that at low RH (A6, ca. 0.63 V – OCV, 50% RH).

suppression in Fig. 8. The Pt oxidation dependence on the holding potential might also depend on the holding time at a high cell potential such as the OCV. In addition, as seen in the results of Fig. 7, the Pt oxidation is accelerated by the load cycles, in which the lower limit voltage is over ca. 0.73 V, such as in the A5, B5 conditions. Uchimura et al. reported that the Pt surface is covered with oxide species during the potential cycling in the potential range from 0.80 V to 0.95 V [19]. Kongkanand and Alsabet have also reported that Pt is more oxidized at higher potentials and longer holding times [21,29]. The Pt dissolution is accelerated when the upper potential limit is greater than 0.8 V [30]. In addition, the presence of O_2 would induce place-exchange [21]. Therefore, these results suggest that the degradation from Pt dissolution is accelerated by both deep oxidation and reduction of PtO, which are caused by both the longer OCV holding and the lower potential limit, respectively (A3 or B3). The reduction of PtO is well known to produce Pt^{2+} [30]. The Pt dissolution during the load cycles occurs particularly in the cathode CL near the membrane side, as shown in Fig. 6(a). The dissolved Pt^{2+} ions diffuse into the membrane and are deposited therein by crossover H_2 from the anode, as shown in Fig. 4(c). These Pt degradation modes in the CL are illustrated in Fig. 8(a). The cell performance in the high current density region decreases remarkably, because the proton paths are extended by the Pt dissolution in the cathode CL near the membrane side (A3 in Fig. 2(b), (d), Fig. 5(b), (c),and Fig. 6(a)).

In the load cycles of condition A5 (low current density, ca. 0.73 V and OCV), the deterioration of the cell performance was suppressed to a greater extent than that in the A3 condition (high current density, ca. 0.63 V and OCV). The comparison of the Pt distribution after the load cycles between conditions A3 and A5 (Fig. 6) indicate that the disappearance of Pt in the CL near the membrane side was suppressed by the low current load of the A5 condition. However, the Pt particle growth was enhanced by the A5 condition, which seems to have been caused by electrochemical Ostwald ripening,. With the lower potential of ca. 0.63 V, more PtO is reduced, which can then diffuse into the membrane, whereas at ca. 0.73 V, less PtO is reduced, and the Pt^{2+} ions tend to be deposited within the CL. In addition, the increase of water-back diffusion is suppressed at the lower current density of 0.1 A cm^{-1}, compared with the higher current density of 0.5 A cm^{-1}, which would otherwise help to carry the Pt^{2+} ions into the membrane. Crossover H_2 may also be suppressed, which otherwise would have caused Pt to be deposited in the membrane at the lower current density. The operating condition with current load affects the amount of water associated with transporting protons [32]; increased humidity has been shown to enhance the H_2 pemeability [33], so we hypothesize that increased load leads to increased H_2 crossover. These Pt degradation modes are consistent with Fig. 6(b) and are illustrated in Fig. 8(b).

In the case of the low RH condition of both A6 and B6, the deterioration of the cell performance and the Q_{PtO} were smaller than these of the other conditions (Figs. 5 and 7). The thicknesses of both the ionomer and the membrane would decrease by lowering the RH, and the water contents would also decrease. The Pt ion transport in the ionomer and membrane would decrease with the shrinking of the water (and ionic) channel networks due to the decrease of the water content in the polymer electrolyte [31]. In addition, the oxidation of Pt was able to be suppressed during the load cycles under the low RH condition, because the Q_{PtO} of B6, simulating A6, during the load cycle at 50% RH was less than the initial value after 12 cycles (Fig. 7). Uchimura et al. have also reported that Pt dissolution is suppressed at low RH (ca. 30% RH) [19]. Therefore, the Pt dissolution and particle growth during the load cycling under lower RH was suppressed (Fig. 6(c), (f)), because the Pt ion transport was low, the oxidation of Pt was limited, and the redeposition of Pt was inhibited, as illustrated in Fig. 8(c). Consequently, we found that low RH operation during load cycling is important in suppressing the Pt degradation from Pt dissolution and Pt particle growth in the cathode CL.

4. Conclusions

We investigated Pt degradation on the GCB support during load cycling as a function of the holding times of OCV/load at 80 °C and 100% RH and found that the Pt degradation depends on the holding time of the OCV during the load cycling. In addition, the Pt dissolved from the cathode electrocatalyst layer was significantly deposited in the membrane during load cycles with longer OCV holding times. We also investigated the effect of both the RH and the current density on the Pt degradation during load cycles with longer OCV holding times and found that the load cycle with lower current density, i.e., higher operating potential, accelerated the Pt particle growth but suppressed the Pt dissolution, and revealed that both the dissolution and the redeposition of Pt were effectively suppressed during load cycles at lower RH due to the decrease of the water content in both ionomer and membrane, which contributes to the poor transport of Pt ions and the suppression of Pt oxidation. Thus, we conclude that the Pt degradation during load cycling is able to be suppressed by operation with a suitable low RH, even for longer OCV holding times, such as during idling and immediately after fuel cell startup.

Acknowledgements

This work was partially supported by funds for the “Research on Nanotechnology for High Performance Fuel Cells” (HiPer-FC) project and the “Superlative, Stable, and Scalable Performance Fuel Cell” (SPer-FC) project from the New Energy and Industrial

Technology Development Organization (NEDO) of Japan.

References

[1] C.A. Reiser, L. Bregoli, T.W. Patterson, J.S. Yi, J.D. Yang, M.L. Perry, T.D. Jarvi, A reverse-current decay mechanism for fuel cells, Electrochem. Solid-State Lett. 8 (2005) A273–A276.

[2] P.T. Yu, W. Gu, R. Makharia, F.T. Wagner, H.A. Gasteiger, The impact of carbon stability on PEM fuel cell startup and shutdown voltage degradation, ECS Trans. 3 (2006) 797–809.

[3] Y.-C. Park, K. Kakinuma, M. Uchida, D.A. Tryk, T. Kamino, H. Uchida, M. Watanabe, Investigation of the corrosion of carbon supports in polymer electrolyte fuel cells using simulated start-up/shutdown cycling, Electrochim. Acta 91 (2013) 195–207.

[4] Y.-C. Park, K. Kakinuma, M. Uchida, H. Uchida, M. Watanabe, Deleterious effects of interim cyclic voltammetry on Pt/carbon black catalyst degradation during start-up/shutdown cycling evaluation, Electrochim. Acta 123 (2014) 84–92.

[5] R.L. Borup, J.R. Davey, F.H. Garzon, D.L. Wood, M.A. Inbody, PEM fuel cell electrocatalyst durability measurements, J. Power Sources 163 (2006) 76–81.

[6] R. Lin, B. Li, Y.P. Hou, J.M. Ma, Investigation of dynamic driving cycle effect on performance degradation and micro-structure change of PEM fuel cell, J. Hydrogen Energy 34 (2009) 2369–2376.

[7] K. Teranishi, K. Kawata, S. Tsushima, S. Hirai, Degradation mechanism of PEMFC under open circuit operation, Electrochem. Solid-State Lett. 9 (2006) A475–A477.

[8] S. Kundu, M. Fowler, L.C. Simon, R. Abouatallah, Reversible and irreversible degradation in fuel cells during open circuit voltage durability testing, J. Power Sources 182 (2008) 254–258.

[9] D.C. Johnson, D.T. Napp, S. Bruckenstein, A ring-disk electrode study of the current/potential behaviour of platinum in 1.0 M sulphuric and 0.1 M perchloric acids, Electrochim. Acta 15 (1970) 1493–1509.

[10] D.A.J. Rand, R. Woods, A study of the dissolution of platinum, palladium, rhodium and gold electrodes in 1 m sulphuric acid by cyclic voltammetry, J. Electroanal. Chem. Interfacial Electrochem. 35 (1972) 209–218.

[11] X. Wang, R. Kumar, D.J. Myers, Effect of voltage on platinum dissolution, Electrochem. Solid-State Lett. 9 (2006) A225–A227.

[12] J.A. Bett, K. Kinoshita, P. Stonehart, Crystallite growth of platinum dispersed on graphitized carbon black, J. Catal. 35 (1974) 307–316.

[13] J.A.S. Bett, K. Kinoshita, P. Stonehart, Crystallite growth of platinum dispersed on graphitized carbon black: II. Effect of liquid environment, J. Catal. 41 (1976) 124–133.

[14] S. Kawahara, S. Mitsushima, K. Ota, N. Kamiya, Deterioration of Pt catalyst under potential cycling, ECS Trans. 3 (2006) 625–631.

[15] S. Mitsushima, S. Kawahara, K. Ota, N. Kamiya, Consumption rate of Pt under potential cycling, J. Electrochem. Soc. 154 (2007) B153–B158.

[16] S. Mitsushima, Y. Koizumi, S. Uzuka, K. Ota, Dissolution of platinum in acidic media, Electrochim. Acta 54 (2008) 455–460.

[17] F. Hiraoka, K. Matsuzawa, S. Mitsushima, Degradation of Pt/C under various potential cycling patterns, Electrocatalysis 4 (2013) 10–16.

[18] M. Uchimura, S.S. Kocha, The Impact of cycle profile on PEMFC durability, ECS Trans. 11 (2007) 1215–1226.

[19] M. Uchimura, S. Sugawara, Y. Suzuki, J. Zhang, S.S. Kocha, Electrocatalyst durability under simulated automotive drive cycles, ECS Trans. 16 (2008) 225–234.

[20] K. Yasuda, A. Taniguchi, T. Akita, T. Ioroi, Z. Siroma, Platinum dissolution and deposition in the polymer electrolyte membrane of a PEM fuel cell as studied by potential cycling, Phys. Chem. Chem. Phys. 8 (2006) 746–752.

[21] A. Kongkanand, J.M. Ziegelbauer, Surface platinum electrooxidation in the presence of oxygen, J. Phys. Chem. C 116 (2012) 3684–3693.

[22] S. Chen, H.A. Gasteiger, K. Hayakawa, T. Tada, Y. Shao-Horn, Platinum-alloy cathode catalyst degradation in proton exchange membrane fuel cells: nanometer-scale compositional and morphological changes, J. Electrochem. Soc. 157 (2010) A82–A97.

[23] B.E. Conway, Electrochemical oxide film formation at noble metals as a surface-chemical process, Prog. Surf. Sci. 49 (1995) 331–452.

[24] H. Imai, K. Izumi, M. Matsumoto, Y. Kubo, K. Kato, Y. Imai, In situ and real-time monitoring of oxide growth in a few monolayers at surfaces of platinum nanoparticles in aqueous media, J. Am. Chem. Soc. 131 (2009) 6293–6300.

[25] G. Jerkiewicz, G. Vatankhah, J. Lessard, M.P. Soriaga, Y.-S. Park, Surface-oxide growth at platinum electrodes in aqueous H_2SO_4 reexamination of its mechanism through combined cyclic-voltammetry, electrochemical quartz-crystal nanobalance, and auger electron spectroscopy measurements, Electrochim. Acta 49 (2004) 1451–1459.

[26] M. Wakisaka, S. Asizawa, H. Uchida, M. Watanabe, In situ STM observation of morphological changes of the Pt(111) electrode surface during potential cycling in 10 mM HF solution, Phys. Chem. Chem. Phys. 12 (2010) 4184–4190.

[27] M. Watanabe, K. Makita, H. Usami, S. Motoo, New preparation method of a high performance gas diffusion electrode working at 100% utilization of catalyst clusters and analysis of the reaction layer, J. Electroanal. Chem. Interfacial Electrochem. 197 (1986) 195–208.

[28] R.N. Carter, B.K. Brady, K. Subramanian, T. Tighe, H.A. Gasteiger, Spatially resolved electrode diagnostic technique for fuel cell applications, ECS Trans. 11 (2007) 423–433.

[29] M. Alsabet, M. Grden, G. Jerkiewicz, Comprehensive study of the growth of thin oxide layers on Pt electrodes under well-defined temperature, potential, and time conditions, J. Electroanal. Chem. 589 (2006) 120–127.

[30] Y. Sugawara, T. Okayasu, A.P. Yadav, A. Nishikata, T. Tsuru, Dissolution mechanism of platinum in sulfuric acid solution, J. Electrochem. Soc. 159 (2012) F779–F786.

[31] W. Bi, Q. Sun, Y. Deng, T.F. Fuller, The effect of humidity and oxygen partial pressure on degradation of Pt/C catalyst in PEM fuel cell, Electrochim. Acta 54 (2009) 1826–1833.

[32] Q. Yan, H. Toghiani, J. Wu, Investigation of water transport through membrane in a PEM fuel cell by water balance experiments, J. Power Sources 158 (2006) 316–325.

[33] S. Takaichi, H. Uchida, M. Watanabe, Distribution profile of hydrogen and oxygen permeating in polymer electrolyte membrane measured by mixed potential, Electrochem. Commun. 9 (2007) 1975–1979.